THE JOURNAL OF PHYSICAL CHEMISTRY A

Article

Cite This: J. Phys. Chem. A 2018, 122, 6292−6302

pubs.acs.org/JPCA

Kinetics and Product Yields of the OH Initiated Oxidation of Hydroxymethyl Hydroperoxide

Hannah M. Allen,[*,†] John D. Crounse,[‡] Kelvin H. Bates,[†] Alexander Paichung Teng,[‡] Mitchell P. Krawiec-Thayer,[¶] Jean C. Rivera-Rios,[§] Frank N. Keutsch,[§] Jason M. St. Clair,[∥,⊥] Thomas F. Hanisco,[⊥] Kristian H. Møller,[#] Henrik G. Kjaergaard,[#] and Paul O. Wennberg[*,‡,▽]

[†]Division of Chemistry and Chemical Engineering, [‡]Division of Geological and Planetary Sciences, and [▽]Division of Engineering and Applied Science, California Institute of Technology, Pasadena, California 91125, United States

[¶]Department of Chemistry, University of Wisconsin Madison, Madison, Wisconsin 53706, United States

[§]Paulson School of Engineering and Applied Sciences and Department of Chemistry and Chemical Biology, Harvard University, Cambridge, Massachusetts 02138, United States

[∥]Joint Center for Earth Systems Technology, University of Maryland Baltimore County, Baltimore, Maryland 21228, United States

[⊥]Atmospheric Chemistry and Dynamics Laboratory, NASA Goddard Space Flight Center, Greenbelt, Maryland 20771, United States

[#]Department of Chemistry, University of Copenhagen, Universitetsparken 5, DK-2100 Copenhagen Ø, Denmark

Supporting Information

ABSTRACT: Hydroxymethyl hydroperoxide (HMHP), formed in the reaction of the C_1 Criegee intermediate with water, is among the most abundant organic peroxides in the atmosphere. Although reaction with OH is thought to represent one of the most important atmospheric removal processes for HMHP, this reaction has been largely unstudied in the laboratory. Here, we present measurements of the kinetics and products formed in the reaction of HMHP with OH. HMHP was oxidized by OH in an environmental chamber; the decay of the hydroperoxide and the formation of formic acid and formaldehyde were monitored over time using CF_3O^- chemical ionization mass spectrometry (CIMS) and laser-induced fluorescence (LIF). The loss of HMHP by reaction with OH is measured relative to the loss of 1,2-butanediol [$k_{1,2\text{-butanediol+OH}} = (27.0 \pm 5.6) \times 10^{-12}$ cm^3 molecule^{-1}s^{-1}]. We find that HMHP reacts with OH at 295 K with a rate coefficient of $(7.1 \pm 1.5) \times 10^{-12}$ cm^3 molecule^{-1}s^{-1}, with the formic acid to formaldehyde yield in a ratio of 0.88 ± 0.21 and independent of NO concentration ($3 \times 10^{10} - 1.5 \times 10^{13}$ molecules cm^{-3}). We suggest that, exclusively, abstraction of the methyl hydrogen of HMHP results in formic acid, while abstraction of the hydroperoxy hydrogen results in formaldehyde. We further evaluate the relative importance of HMHP sinks and use global simulations from GEOS-Chem to estimate that HMHP oxidation by OH contributes 1.7 Tg yr^{-1} (1−3%) of global annual formic acid production.

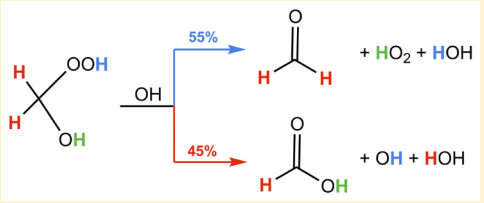

INTRODUCTION

Hydroperoxides significantly contribute to the chemistry of the atmosphere because of their high reactivity. These species alter the atmosphere's oxidative potential by acting as a reactive sink and transported reservoir of HO_x.[1−3] They act as oxidants of SO_2 in the aqueous phase to produce SO_4^{2-}, thereby reducing air quality and visibility.[4,5] In addition, hydroperoxides have been implicated in the inhibition of certain peroxidase enzymes essential to plant function,[6,7] although some studies note that under certain conditions, exposure to ozone can increase plant resistance to oxidative stress from hydroperoxides.[8,9]

Hydroxymethyl hydroperoxide ($HOCH_2OOH$, HMHP) is among the hydroperoxides observed in significant abundance in the atmosphere. Reported concentrations of HMHP vary considerably, but typically fall in the low ppbv range during the summer and have been reported up to 5 ppbv over forested regions.[10−13] Recently, HMHP concentrations were measured during the SEAC^{4}RS (Studies of Emissions, Atmospheric Composition, Clouds, and Climate Coupling by Regional Surveys) flight campaign traversing across the southeastern United States between August 6 and September 23, 2013. HMHP mixing ratios varied considerably depending on location and altitude, but within the boundary layer, the average HMHP mixing ratio was 0.25 ppbv with a maximum of 4.0 ppbv (Figure 1).

HMHP forms when terminal alkenes react with ozone in the presence of water vapor.[14−20] Upon attack by O_3, the alkene fragments into a carbonyl and an energy-rich intermediate, which may be collisionally stabilized to form the C_1 Criegee intermediate (CH_2OO). The C_1 Criegee intermediate then

Received: May 14, 2018
Revised: July 2, 2018
Published: July 11, 2018

DOI: 10.1021/acs.jpca.8b04577
J. Phys. Chem. A 2018, 122, 6292−6302

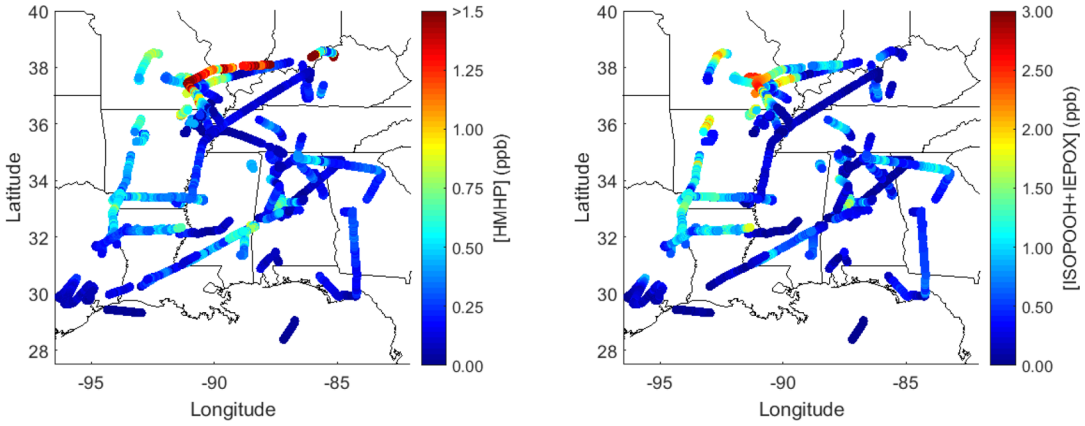

Figure 1. HMHP (left) and isoprene hydroxy hydroperoxide and epoxydiol (ISOPOOH + IEPOX, right) mixing ratios during the summer 2013 SEAC[4]RS flight campaign in the southeastern United States. ISOPOOH and IEPOX result from the OH oxidation of isoprene and are therefore indicative of regions with high isoprene mixing ratios. The average HMHP mixing ratio was 0.25 ppbv but reached above 1 ppbv on several occasions during the campaign. HMHP mixing ratios were often correlated with co-products of one of its precursor species, isoprene, as assessed by ISOPOOH + IEPOX.

reacts with a water-vapor monomer or dimer (n = 1,2) to form HMHP.

$$CH_2OO + (H_2O)_n \rightarrow HOCH_2OOH + (H_2O)_{n-1} \quad (1)$$

Thus, ozonolysis of alkenes with terminal double bonds (such as isoprene and β-pinene as well as simpler alkenes such as ethene, propene, and 1-butene) contribute to HMHP formation (e.g., Figure 1).

Understanding the relative rates of production and removal mechanisms of HMHP is key to assessing its lifetime and importance in the atmosphere. HMHP undergoes three major atmospheric removal processes: photolysis, deposition, and reaction with the hydroxyl radical. Numerous studies investigating the spectroscopic properties of HMHP have concluded that photolysis is likely to be less significant than other atmospheric-loss processes (photolysis rate of $J \approx 1 \times 10^{-6}$ s^{-1} under typical atmospheric conditions).[21−25] HMHP is highly water-soluble (Henry's Law constant of $H \approx 10^6$ M atm^{-1})[26] and is therefore highly susceptible to rainout and dry deposition.[13] Reaction with OH is expected to be an important sink of HMHP, with three possible H-abstraction pathways: abstraction of (a) the hydroperoxidic hydrogen, (b) the alkyl hydrogen, and (c) the alcoholic hydrogen.[27] These pathways lead to the formation of formic acid (HCOOH) or formaldehyde (HCHO) with OH or HO_2 radicals as byproducts, respectively. However, the rate coefficient for this reaction has not been previously reported.

In this study, we investigate the reaction of HMHP with OH. HMHP was oxidized by OH in an environmental chamber, and the decay of the hydroperoxide was monitored over time using CF_3O^- chemical ionization mass spectrometry (CIMS). Product yields of formic acid and formaldehyde were characterized by CIMS and by laser-induced fluorescence (LIF), respectively. The yield of formic acid was further characterized under varying NO concentrations to assess the HMHP + OH oxidation pathways. HMHP sinks and the impact of HMHP oxidation on global formaldehyde and formic acid concentrations are interpreted in the context of simulations using GEOS-Chem to evaluate the global importance of HMHP oxidation.

EXPERIMENTAL METHODS

Instrumentation. Chemical ionization mass spectrometry (CIMS) is a versatile and robust technique for detecting a variety of atmospheric compounds, including hydroperoxides. Reagents and oxidation products in this work were monitored using a compact time-of-flight CIMS (ToF-CIMS, Tofwerk/Caltech) that employs a CF_3O^- reagent ion for sensitive detection of gas-phase organic acids and multifunctional organic compounds. The CF_3O^- CIMS technique has been described in detail in Crounse et al.,[28] Paulot et al.,[29] and St. Clair et al.[30]

Briefly, the reagent ions form by passing 380 sccm of 1 ppm of CF_3OOCF_3 in N_2 through a cylindrical ion source containing a layer of radioactive polonium-210 (NRD LLC, ≤ 10 mCi). The sample air is diluted with dry N_2 (1750 sccm) in a Pyrex glass flow tube with a hydrophobic coating (Fluoropel 801A, Cytonix) that is maintained at a pressure of 35 mbar. The diluted sample air then mixes with the reagent ions, which selectively ionize analytes by forming ion clusters (m/z = analyte mass + 85) or fluoride transfer ions (m/z = analyte mass + 19), the dominance of which depends on the acidity and fluoride affinity of the target analyte. Product ions are transferred through a pinhole orifice and a conical hexapole ion guide to the time-of-flight mass spectrometer chamber. Compounds are separated in the mass spectrometer based on differences in their mass-to-charge ratio as they accelerate through the instrument.

The ToF-CIMS provides 10 Hz resolution data for masses between m/z 19 and 396. In this study, HMHP was monitored at m/z 149 (HMHP·CF_3O^-); the relative rate partner, 1,2-butanediol, was monitored at m/z 175 (1,2-butanediol·CF_3O^-); formic acid (FA) was monitored at m/z 65 (FA_{-H}·HF); and bis-HMP (bis-hydroxymethyl peroxide, $HOCH_2OOCH_2OH$) was monitored at both m/z 113 (bis-HMP_{-H}·HF) and m/z 179 (bis-HMP·CF_3O^-). All observed ion signals were normalized to the sum of the reagent anion signal ($^{13}CF_3O^-$ isotope at m/z 86) and the water signal (m/z 104, H_2O·$^{13}CF_3O^-$ isotope) to account for fluctuations in the reagent ion concentration. Detection limits for the ToF-CIMS are typically 10 pptv for a 1 s integration period.

In addition to the ToF-CIMS, other instruments were employed to assess concentrations of formaldehyde, NO, and

DOI: 10.1021/acs.jpca.8b04577
J. Phys. Chem. A 2018, 122, 6292−6302

Table 1. Summary of Conditions Used in HMHP Oxidation Experiments[a]

exp.	$[HMHP]_0$	$[OH\ source]_0$[b]	$[1,2\text{-}BD]_0$	initial $[NO]_0$	% HMHP ox.	objective
1	150	190	80	475	35	kinetics
2	90	200	15	460	40	kinetics
3	35	190	15	160	55	kinetics
4	165	100	—	445	30	yields
5	55	45	—	20	45	NO_x dep.
6	70	30	—	500	30	NO_x dep.
7	20	20	—	20	35	NO_x dep.
8	10	60	—	25	50	NO_x dep.
9	20	120	—	530	40	NO_x dep.

[a]Mixing ratios are given in ppbv. Experiments were performed at ambient laboratory temperature (295 K) and pressure (745 Torr). [b]The OH source was methyl nitrite for kinetics and NO_x dep. experiments and isopropyl nitrite for the yields experiment.

O_3 over the course of the experiment. Formaldehyde product yields were characterized by the NASA In Situ Airborne Formaldehyde (ISAF) instrument.[31] Briefly, the ISAF instrument employs a pulsed tunable fiber laser for LIF detection of HCHO. The laser operates at 353 nm, exciting a single rotational transition of the A−X band in HCHO. The instrument has a 10 Hz sampling frequency that is averaged to 1 s, at which the precision is typically better than 20% above 100 pptv. NO_x and O_3 concentrations throughout the experiment were monitored with an NO_x monitor (Teledyne 200 EU) and an O_3 monitor (Teledyne 400E). All instruments sampled the chamber from a sampling loop of 0.635 cm OD PFA tubing.

HMHP Synthesis. A new method for synthesizing HMHP was performed in this study. The method is based on a technique described in Bauerle and Moortgat,[22] in which formaldehyde vapor is passed through hydrogen peroxide to generate HMHP. Here, HCHO was prepared by gently heating crystalline paraformaldehyde (Sigma-Aldrich) and passing the resulting vapor through two successive cryotraps at −65 and −196 °C to collect impurities and condense HCHO, respectively. A small (∼10 sccm) flow of N_2 was then passed over the collected HCHO, held at −65 °C, and bubbled through urea hydrogen peroxide (Sigma-Aldrich, 97%, 1100 mg) in dichloromethane (DCM, 30 mL) held in a −30 °C cold bath. After approximately 5 min of flow, the −30 °C bath was removed, and the reaction mixture was allowed to warm to room temperature. HMHP formed from this method in a relative yield of approximately 4:1 HMHP to bis-HMP and with small amounts of HCHO and H_2O_2 also present (as determined by gas-phase analysis of an evaporated droplet of the synthetic mixture). Note that previous synthesis using a similar method found significant safety hazards upon concentration of the hydroperoxide product (e.g., Fry et al.[23]).

Chamber Experiments. Experiments on HMHP + OH oxidation were conducted in a small environmental chamber. The chamber consisted of a 1 m^3 fluorinated ethylene propylene copolymer bag (Teflon-FEP, DuPont) within an enclosure equipped with UV lights (8 Sylvania 350 blacklights) and has been described previously.[32−34] The chamber was prepared by multiple flushes of dry air between successive experiments. Table 1 provides a description of experimental conditions.

Reagents were added to the chamber sequentially after flushing the chamber bag with dry air and filling it to near 50% with zero air. NO (1993 ± 20 ppmv in N_2, Matheson) was prepared by filling an evacuated 500 cm^3 glass bulb to the desired pressure and backfilling with N_2 before adding to the chamber. Next, 1,2-butanediol (1,2-BD, ≥ 98%, Sigma-Aldrich) was added as a relative rate partner by flowing dry air at 20 L min^{-1} over a small drop of the diol placed in a glass vial. 1,2-Butanediol was chosen as a relative rate partner, because it is sensitively detected with the CF_3O^- CIMS technique and has a known OH reaction rate constant that is expected to be similar to that of HMHP + OH. A method similar to that outlined in Taylor et al.[35] was used to synthesize the HO_x source used in this study, methyl nitrite (CH_3ONO). Approximately 200 ppbv of CH_3ONO was added to the chamber via serial dilution of vapor contained in a 500 cm^3 glass bulb. Finally, HMHP was added to the chamber by first evaporating and cryocollecting the sample to remove high volatility impurities generated from the synthesis. Zero air was passed for 10−30 s over a three way vial containing approximately 0.5−1.2 mL of synthesized HMHP in DCM, and HMHP was subsequently trapped on PFA tubing submerged in a cold bath at −80 °C. Upon removal of the bath, the cryotrapped sample was flushed into the chamber with zero air for approximately 20 min until the remainder of the chamber volume was filled. H_2O_2 and HCHO were present in the chamber in minor amounts (∼5 and ∼2% relative to HMHP, respectively) from the HMHP synthetic mixture described above.

Photo-oxidation was initiated after stabilization of the CIMS signals (15 to 50 min). The UV lights were turned on to generate OH radicals via

$$CH_3ONO + h\nu \xrightarrow{O_2} HO_2 + NO + HCHO \quad (2a)$$

$$HO_2 + NO \rightarrow OH + NO_2 \quad (2b)$$

This process produced OH concentrations that were typically ∼50 times greater than average atmospheric levels. Oxidation lasted until the OH precursor was depleted (∼1 h), utilizing three of the chamber's UV lights. Approximately 30−50% of HMHP was oxidized.

The chamber was prepared in a very similar manner for all experiments, with a few notable exceptions. For Exps. 4−9, 1,2-butanediol was not added to the chamber to minimize any interference in the product yield because of oxidation of this species. For Exp. 4, in which HCHO was measured, isopropyl nitrite was used as the OH source to preclude HCHO interference from CH_3ONO photolysis. In addition, a series of experiments were conducted to assess the NO_x dependence of the formic acid yield. In these experiments, a further step was taken to purify HMHP from the reaction mixture. The solvent and high volatility impurities were removed first by either flowing zero air over the reaction mixture at −80 °C or by

DOI: 10.1021/acs.jpca.8b04577
J. Phys. Chem. A 2018, 122, 6292−6302

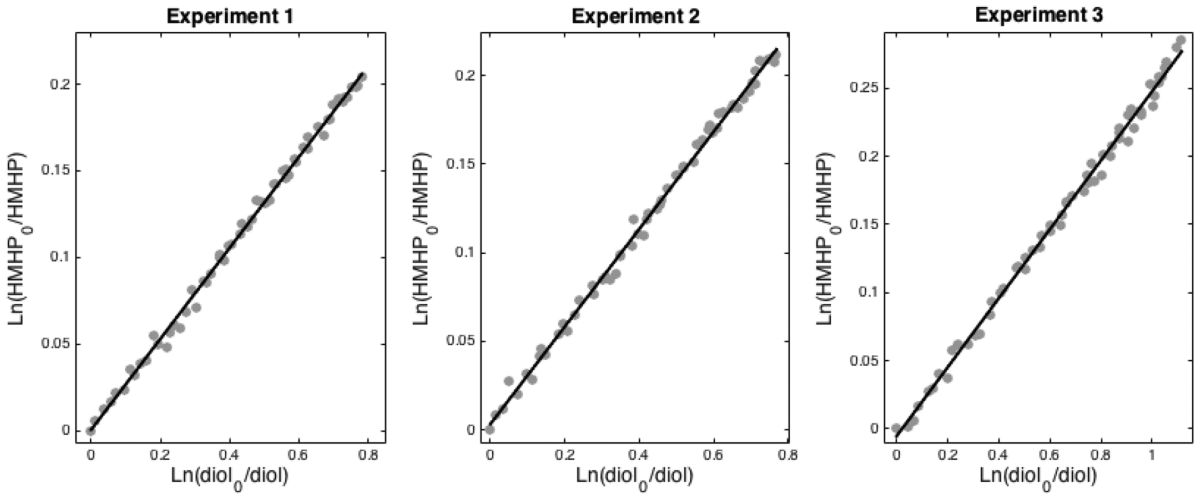

Figure 2. Fit (black) of the natural logarithmic decay of HMHP vs 1,2-butanediol (diol) during oxidation. HMHP and 1,2-butanediol data are measured at ToF-CIMS signals m/z 149 and 175, respectively, and averaged over 30 s between 15 and 45 min into the oxidation. The relative decay is used to determine the HMHP + OH oxidation rate.

placing the reaction mixture under vacuum. To isolate HMHP from the lower volatility bis-HMP synthetic byproduct, the remaining reaction mixture was collected in a cold trap, and HMHP was eluted at a temperature of −15 °C.

Calibration. A gravimetric technique was used to calibrate the ToF-CIMS for formic acid. A commercially available formic acid standard (Sigma-Aldrich, 98%) was dissolved in water (1% w/w solution) and volatilized into the chamber by flowing a known amount of dry air over the sample until it had completely evaporated. The dry and water-dependent sensitivities were determined by addition of varying concentrations of water vapor to the sample before it entered the CIMS instrument. This water-vapor calibration was applied to the ToF-CIMS formic acid signal during analysis. Because there is no commercially available standard, the absolute sensitivity of HMHP could not be determined. Using the synthetic sample, the change in HMHP sensitivity due to changing water vapor concentrations was determined in a manner similar to that for formic acid. This relative calibration was used in analysis of the ToF-CIMS HMHP signals. The bis-HMP ToF-CIMS sensitivity relative to HMHP was estimated from ion−molecule collision rates, which were parametrized from the calculated dipole moment and polarizability of the neutral molecules.[36−38] See the Supporting Information for further details of the ToF-CIMS calibration procedures. HCHO instrument sensitivity for ISAF was determined via calibration against standard additions of a commercially available HCHO standard to zero air. See Cazorla et al.[31] for further details of the ISAF calibration procedure.

Theoretical Methods. Reaction rate constants for the unimolecular reactions are calculated with the approach by Møller et al.[39] using multiconformer transition state theory with Eckart tunneling. The electronic energies are calculated using coupled cluster methods in Molpro2012, while zero-point vibrational energy corrections and partition functions are calculated using density functional theory in Gaussian 09.[40,41] Rice−Ramsperger−Kassel−Marcus (RRKM) modeling of selected reactions is done using the Master Equation Solver for Multi-Energy well Reactions (MESMER) and the Multi-Well program suite.[42,43] See Supporting Information for details.

RESULTS AND DISCUSSION

HMHP + OH Rate Coefficient. The HMHP + OH reaction rate coefficient (k_{HMHP}) relative to that of 1,2-butanediol + OH (k_{diol}) was determined at ambient temperature using data from experiments 1−3 (Table 1). The rate coefficient of 1,2-butanediol with OH is (27.0 ± 5.6) × 10^{-12} cm^3 $molecule^{-1}s^{-1}$ at T = 296 K.[44] To obtain the rate constant for HMHP + OH relative to that of 1,2-butanediol + OH, the natural logarithm of the HMHP mixing ratio (normalized to the initial concentration) was plotted as a function of the natural logarithm of the normalized 1,2-butanediol mixing ratios over the course of oxidation (Figure 2). The slope of a linear regression analysis incorporating error in both dimensions[45] gives the reaction rate of HMHP relative to 1,2-butanediol (k_{HMHP}[OH]/k_{diol}[OH]) for each experiment. Table 2 lists the relative rates k_{HMHP}/k_{diol} and gives a recommended rate constant for the OH oxidation of HMHP (calculated by taking a mean of all experimental runs weighted by their respective uncertainties).

Table 2. Relative Rate of HMHP + OH to 1,2-Butanediol + OH[a] at 295 K for Experiments 1−3 and Derived Absolute HMHP + OH Rate Coefficient[b]

experiment 1	experiment 2	experiment 3	rate coefficient
0.262 ± 0.008	0.275 ± 0.011	0.253 ± 0.015	7.1 ± 1.5

[a](k_{HMHP}/k_{diol}). [b](10^{-12} cm^3 $molecule^{-1}s^{-1}$). Uncertainties are 1σ standard deviations from measurement uncertainties; the rate coefficient also includes error in the 1,2-butanediol + OH rate coefficient.

The uncertainty for all experiments is dominated by the 20% uncertainty in the 1,2-butanediol rate constant. Other appreciable sources of error arose from the loss of HMHP on the walls of the chamber, equilibration of the ToF-CIMS signals, and the error in the linear fit. To account for uptake of HMHP to the chamber walls, a first-order loss rate of (0.8 ± 0.2) × 10^{-5} s^{-1} was used in the data analysis (5% correction to the HMHP data). This rate was determined by filling the chamber with 12 ppbv of HMHP and monitoring the decay of the signal in the dark. The signal from 1,2-butanediol was also corrected for minor wall loss (0.5% correction). In addition,

DOI: 10.1021/acs.jpca.8b04577
J. Phys. Chem. A 2018, 122, 6292−6302

HMHP mixing ratios were corrected for a minor loss due to photolysis ($J = 8.5 \times 10^{-7}$ s^{-1}, calculated from measured light flux in the chamber and from quantum yields and cross sections in Sander et al.;[46] total correction of <1%). Data from $t < 15$ and $t > 45$ min into the oxidation was not used in Figure 2 or to evaluate the kinetics of HMHP + OH (5% correction to the rate constant). The first few minutes of oxidation were disregarded to minimize error due to equilibration of sampling surfaces, such as chamber and tubing walls. At long oxidation times, most of the OH precursor had been depleted, causing photochemical reactions to slow and making relative loss to the chamber walls substantial.

HMHP Oxidation Products. Experiments to determine the yields of formic acid and HCHO from HMHP oxidation were conducted in a manner similar to that of the kinetics experiments. A constant correction factor of 0.10 × [HMHP] was subtracted from all HCHO signals to account for an estimated HMHP decomposition in the ISAF HCHO instrument (see the Supporting Information for more details). HMHP and formic acid were corrected for wall loss by applying the experimentally derived wall loss rates to the data. Under the experimental conditions, formic acid wall loss is comparable to wall production, the sum of which is minor compared to total formic acid production from HMHP (~2.5%). The loss of formic acid and HCHO because of the reaction with OH was accounted for as described by eq VI of Atkinson et al.[47] (1.5% for FA and up to 15% for HCHO; see the Supporting Information). HCHO was also corrected for loss due to photolysis ($J = 1.7 \times 10^{-5}$ s^{-1}, calculated from measured light flux in the chamber and from quantum yields and cross sections in Sander et al.;[46] up to 5% correction). As previously discussed, bis-HMP was present in the chamber during the oxidation experiment. Observed formic acid mixing ratios were corrected for bis-HMP + OH production of formic acid, assuming that bis-HMP oxidation produces 2 equiv of formic acid. This process is calculated to produce up to 40% of total formic acid, using a bis-HMP + OH rate coefficient that is 35% that of HMHP + OH as determined from the kinetics experiments (see the Supporting Information).

The ratio of the formic acid to the HCHO yield was found in Exp. 4 by comparing the change in these species during the oxidation period and using a linear regression that accounts for error in both dimensions.[45] These yields are assessed from data taken between $t = 15$ min and $t = 45$ min into the oxidation, to minimize error due to equilibration of sampling surfaces and to loss on chamber walls. The results of the linear regression analysis is presented in Figure 3. The reaction of HMHP with OH produces formic acid and HCHO in comparable amounts with a formic acid to HCHO product ratio of 0.88 ± 0.21. The reported uncertainty arises from the errors in the calibration of the ToF-CIMS data and from corrections due to HMHP interference in ISAF, product loss due to reaction with OH, and bis-HMP + OH production of formic acid as outlined above, as well as from uncertainty in the line of best fit.

To assess carbon closure from HMHP + OH, an upper limit to the HMHP sensitivity was estimated using the yield experiment. As discussed previously, the absolute sensitivity of the ToF-CIMS to HMHP is not well-known. Assuming that formic acid and HCHO are the only two products from HMHP + OH, the total change in HMHP mixing ratios over the experiment was assumed to be equal to the change in the sum of the two products. This mixing ratio was then used to derive an upper limit to the expected HMHP sensitivity on the ToF-CIMS. Using this sensitivity, we calculate HMHP yields from ethene ozonolysis experiments conducted in the 1 m^3 chamber (see the Supporting Information). Within error, these yields are the same as those reported by Hasson et al.,[48] consistent with formic acid and HCHO as the only major products from the reaction of HMHP with OH.

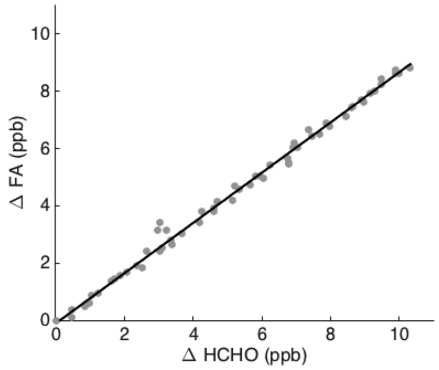

Figure 3. Production of formic acid (FA) compared with that of HCHO. Formic acid was measured on the ToF-CIMS at m/z 65, and the HCHO data are from ISAF during Experiment 4. The signals are corrected for losses outlined in the text and averaged over 30 s between 15 and 45 min into the oxidation. The black line indicates the best fit to the data.

As shown in Figure 4, formic acid can form following abstraction of the methyl, alcoholic, or hydroperoxy hydrogens. Abstraction of the hydroperoxide H (pathway (a) in Figure 4) leads to the formation of the hydroxy peroxy radical ($HOCH_2OO$). This radical forms with excess energy from the abstraction and may react unimolecularly to lose HO_2 before undergoing collisional thermalization. Following stabilization, the radical has two possible subsequent reaction paths: unimolecular thermal decomposition to HO_2 and HCHO or bimolecular reaction with NO forming the hydroxy alkoxy radical ($HOCH_2O$), which then decomposes to H and formic acid.[21,27,49,50] Pathway (b) leads directly to formation of formic acid. Francisco and Eisfeld[27] performed a theoretical calculation of HMHP + OH and concluded that pathway (b) dominates the reactivity, as they find that this pathway has the lowest reaction barrier. However, no previous experimental evidence has been reported to test these conclusions, and the calculated barrier for ROOH abstraction is much higher than expected on the basis of the reaction kinetics of other organic peroxides. Abstraction of the alcoholic H of HMHP (pathway (c) in Figure 4) also leads to the formation of the $HOCH_2OO$ radical because of a favorable 1,4-H shift; however, this pathway is expected to be minor in comparison to pathways (a) and (b) because of the difference in known ROH vs ROOH abstraction rates.[51]

The formic acid yield was evaluated as a function of NO mixing ratio, which was varied between a few and more than 500 ppbv [~$(0.003-1.5) \times 10^{13}$ molecules cm^{-1}]. Results from these experiments indicate that there is no obvious dependence of the formic acid yield on the amount of NO present (Figure 5). The initial concentration of NO used in these experiments is listed in Table 1; note that NO concentrations in the chamber generally decrease from this value as the oxidation proceeds. The imprecision in the measured yield is a result of the experimental challenges described above. These include the need to accurately describe the wall loss of the hydroperoxides and formic acid as well as

DOI: 10.1021/acs.jpca.8b04577
J. Phys. Chem. A 2018, 122, 6292−6302

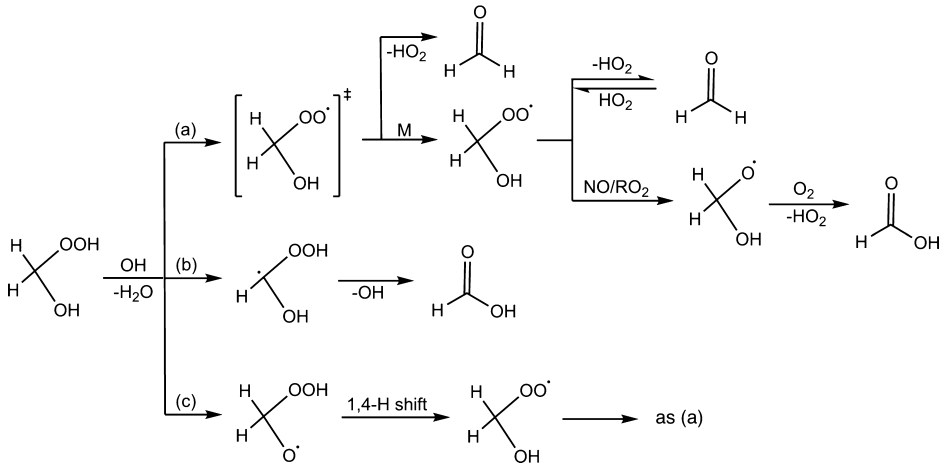

Figure 4. Mechanism of HMHP gas-phase oxidation by OH. HMHP oxidation may proceed via one of three pathways: (a) abstraction of the hydroperoxidic hydrogen, (b) abstraction of the methyl hydrogen, and (c) abstraction of the alcoholic hydrogen. In theory, pathway (a) may further bifurcate depending on the NO concentration.

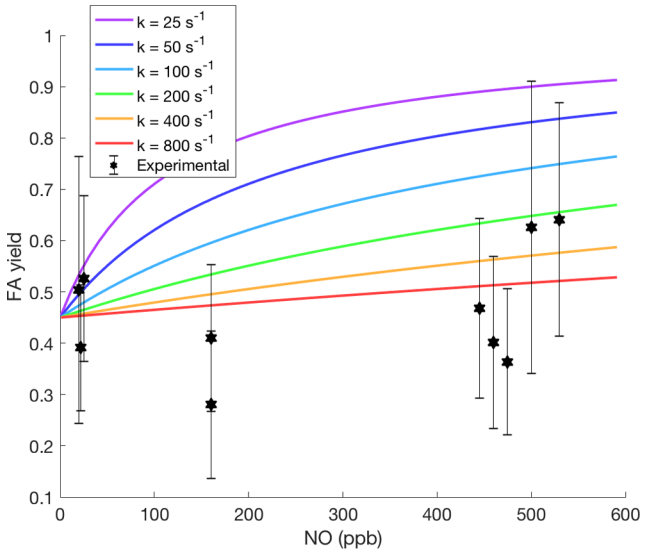

Figure 5. Correlation of experimental formic acid (FA) yields with derived uncertainty against initial NO mixing ratio. The formic acid yields do not appear to exhibit a dependence on NO, indicating that the unimolecular HO_2-loss rate is faster than expected from literature reports of thermalized $HOCH_2OO$. These yields are compared with those predicted by a box model using a range of unimolecular $HOCH_2OO$ decomposition rates.

errors in accounting for formic acid production from the oxidation of bis-HMP.

The lack of dependence of the formic acid yield on [NO] shows some discrepancy with the predicted yield from reported unimolecular $HOCH_2OO$ decomposition rates. The decomposition rate of $HOCH_2OO$ has been measured to be quite slow, between 1.5−140 s^{-1} at T = 298 K (see Table 3). Even at the fastest experimentally determined decomposition rate, reaction of the peroxy radical with NO would be expected to be competitive (pseudo first-order rate of 120 s^{-1} at highest NO concentrations) with the unimolecular decomposition. As a result, the formic acid yield would be expected to depend on NO, such that higher NO concentrations would predict greater formic acid yield. Shown in Figure 5 are kinetic box model calculations of the predicted formic acid yield when using unimolecular HO_2-loss rates of 25, 50, 100, 200, 400, and 800 s^{-1} (see Supporting Information). The lack of clear dependence on [NO] suggests that the unimolecular decomposition in these experiments occurs at a rate of greater than a few hundred per second at T = 295 K.

Table 3. Reported Rates of $HOCH_2OO$ Decomposition

study	method	rate (s^{-1})	notes
Su et al., 1979[21]	FTIR	1.5	kinetic simulations with experimental data
Veyret et al., 1982[52]	FTIR	30	kinetic simulations with experimental data
Barnes et al., 1985[53]	FTIR	20	measured loss of HO_2 by proxy (HO_2NO_2)
Veyret et al., 1989[54]	UV	125	kinetic fits to loss of HO_2
Burrows et al., 1989[55]	UV/FTIR	140	kinetic simulations of measured K_{eq}
Hermans et al., 2005[56]	MC-TST[a]	200	
Morajkar et al., 2013[57]	cw-CRDS	55	measured loss of HO_2
this study	MC-TST[a]	440	see Supporting Information

[a]Multifconformer transition state theory.

The difference between the rate for unimolecular loss of HO_2 inferred in this study with those previously reported (Table 3) likely reflects some combination of experimental error and differences in the initial energy distribution of the $HOCH_2OO$ radicals. Most of the measured rates shown in Table 3 were determined by observing the loss of HCHO, HO_2, or the formation of the $HOCH_2OO$ radical in the presence of excess formaldehyde both with and without NO_x present. Morajkar et al.,[57] for example, inverted the time dependence of HO_2 to diagnose two rate coefficients: the initial rapid loss of HO_2 is used to assess the rate of formation of $HOCH_2OO$ (the inverse of the unimolecular decomposition), and the second subsequent and much slower loss is used to infer the equilibrium coefficient; the proper assignment of the HO_2 dynamics is thus complicated. Theoretical calculations of $HOCH_2OO$ decomposition performed in this study suggest a significantly faster decomposition rate of 440 s^{-1} at 298 K (see Supporting Information).

The rate of decomposition of $HOCH_2OO$ is also likely sensitive to how this species is formed. In the studies shown in Table 3, $HOCH_2OO$ is produced cold via the association

DOI: 10.1021/acs.jpca.8b04577
J. Phys. Chem. A 2018, 122, 6292−6302

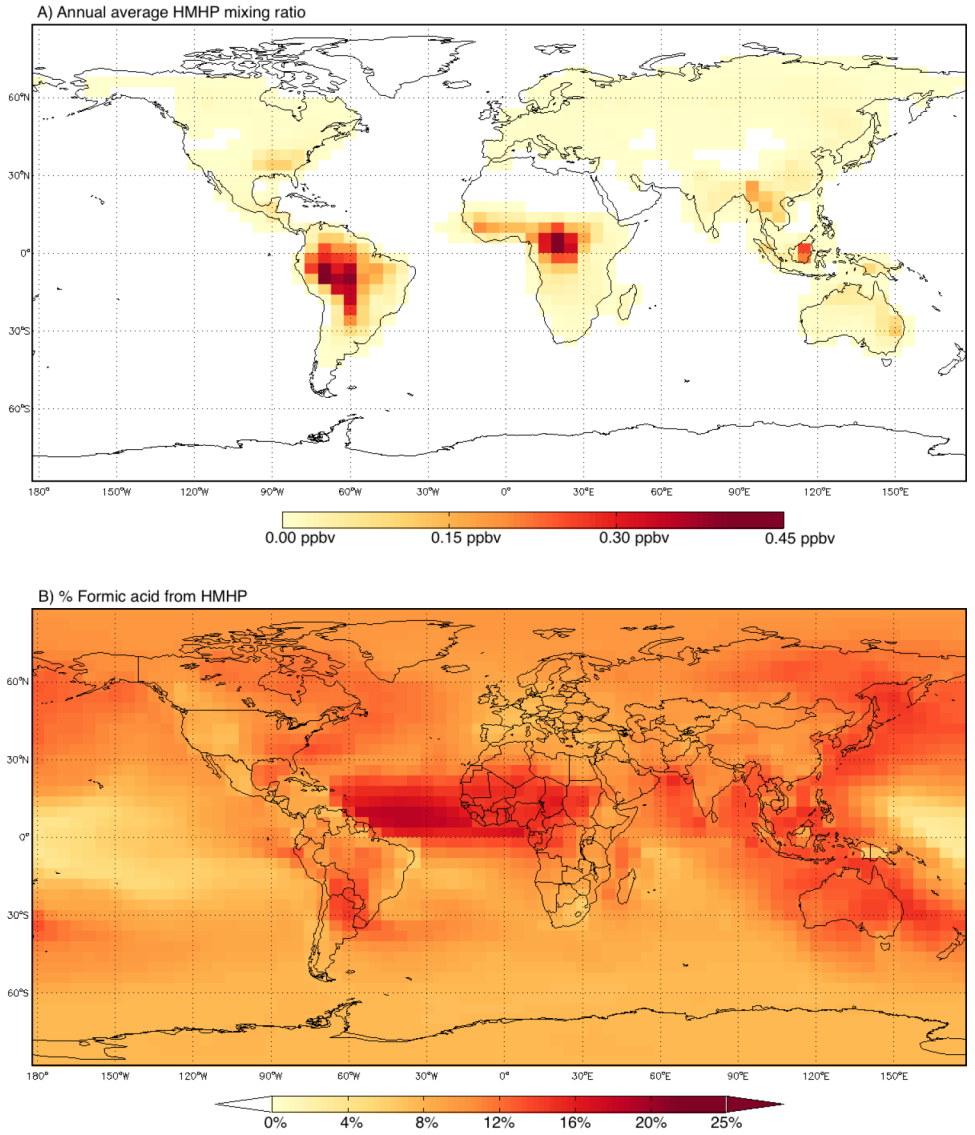

Figure 6. Annual average global distribution of HMHP and formic acid for 2014 from the updated HMHP and isoprene mechanism. (A) HMHP mixing ratios between 0−0.5 km above the surface and (B) percent of modeled formic acid resulting from HMHP oxidation between 0−1 km.

reaction of HCHO + HO_2. In contrast, when $HOCH_2OO$ forms as a result of HMHP oxidation, some of the reaction exothermicity will be deposited in the peroxy radical, speeding the rate of decomposition. RRKM simulations of the experimental system (see Supporting Information) suggest that, provided that less than 8 kcal mol^{-1} of the exothermicity deposits into H_2O, all of the $HOCH_2OO$ will decompose to formaldehyde and HO_2 before collisional stabilization. Hence, we interpret the lack of NO-dependence of the formic acid yields as implying that the $HOCH_2OO$ formed from HMHP oxidation by OH decomposes at a rate sufficiently high such that formaldehyde is the only product following abstraction of the hydroperoxide hydrogen, both for conditions of this experiment and those relevant in the atmosphere.

From these results, we suggest that, exclusively, pathway (a) leads to formaldehyde formation, while pathway (b) leads to formic acid formation, with branching ratios of 0.55 and 0.45, respectively. By comparison, Vaghjiani and Ravishankara[58] studied the OH oxidation of HMHP's homologue, methyl hydroperoxide (MHP, CH_3OOH). At room temperature, MHP reacts with OH at a rate about 0.75 times that of HMHP with OH [$k_{MHP+OH} = (5.4 \pm 0.4) \times 10^{-12}$ cm^3 $molecule^{-1}s^{-1}$] and with hydroperoxide and alkyl abstraction branching ratios of 0.70 and 0.30, respectively.[58] These branching ratios give very similar ROOH abstraction rates between HMHP and MHP and suggest that the faster HMHP + OH kinetics results from an enhanced methyl abstraction reaction rate.

Atmospheric Implications. Consideration of the three major atmospheric-loss processes for HMHP (deposition, OH reaction, and photolysis) allows for the estimation of its total lifetime and the relative contribution of each loss mechanism. For example, HMHP fluxes and OH concentrations were measured in the southeastern United States during the Southern Oxidant and Aerosol Study (SOAS) in summer 2013. During the campaign, the diurnal-average OH concentration was typically around 1×10^6 molecules cm^{-3} but on some days peaked at levels more than twice as large.[59] Our measured HMHP + OH rate coefficient produces a lifetime with respect to oxidation by OH, τ_{OH}, of between 15 and 40 h. By comparison, the diurnal average of the cloud-free atmospheric photodissociation rate at ground level is calculated by the Tropospheric Ultraviolet−Visible (TUV)

DOI: 10.1021/acs.jpca.8b04577
J. Phys. Chem. A 2018, 122, 6292−6302

radiation model (NCAR/ACD) to be 1.8×10^{-6} s^{-1}. This value gives an HMHP lifetime of about 1 week against photolysis in the boundary layer. Using the dry deposition velocity of HMHP measured by Nguyen et al.[13] during SOAS (4 cm s^{-1}) and an assumed mixed layer depth of 1.5 km, the lifetime of HMHP with respect to dry deposition is 10 h. For these conditions, oxidation by OH accounts for between approximately 20−40% of HMHP loss.

Global Modeling. To investigate the global importance of HMHP chemistry, we simulate the production and fate of HMHP using the chemical transport model GEOS-Chem. GEOS-Chem is a three-dimensional model of tropospheric chemistry driven by assimilated meteorological observations from the NASA Goddard Earth Observing System (GEOS).[60] The model includes isoprene oxidation chemistry,[61] which has been extensively updated to reflect recent mechanistic studies.[32,33,62−65] We have updated the GEOS-Chem mechanism to include HMHP yields from alkene ozonolysis taken from Neeb et al.,[66] Hasson et al.,[67] and Nguyen et al.[63] as well as HMHP loss due to deposition from Nguyen et al.,[13] photolysis based on Roehl et al.,[24] and OH oxidation from the results presented in this study. We have assumed that the HMHP + OH rate coefficient exhibits the same temperature dependence as the reaction of MHP with OH. The simulations reported here were conducted for the year 2014 on a global 4 × 5° latitude by longitude grid, following a 1 year model spin up, and use model version 10−01 with GEOS-FP meteorology.

HMHP forms in substantial quantities in regions with large biogenic VOC emissions. Globally, HMHP has a total annual production of 12.4 Tg yr^{-1}, with 8.6 Tg yr^{-1} of that from the approximately 7.5% of isoprene that reacts with ozone. The annually averaged boundary layer (z = 0−0.5 km) HMHP mixing ratios are typically around 0.1 ppbv but reach up to 0.5 ppbv in the heavily forested regions of South America and Africa where isoprene emissions are largest (Figure 6A). In the southeastern United States, the GEOS-Chem predicted average HMHP mixing ratios for the summer of 2013 in the boundary layer are around 0.3 ppbv (see the Supporting Information). By comparison, the average HMHP mixing ratio observed in the boundary layer in the southeastern United States during the SEAC^{4}RS flight campaign in summer 2013 was 0.25 ppbv and reached as high as 4.0 ppbv (Figure 1).

As products of HMHP oxidation, global concentrations and distributions of formic acid and HCHO are altered when HMHP is included in the model. The model predicts that 40% of HMHP is lost to OH, thereby producing 1.7 Tg yr^{-1} of formic acid, with the remaining loss due to deposition (52%) and photolysis (7%). The magnitude of the OH oxidation pathway is substantial in the lower atmosphere; in certain locations, up to 25% of local formic acid mixing ratios is simulated to arise from the oxidation of HMHP (Figure 6B). However, the global production of formic acid from HMHP + OH is small compared with previous GEOS-Chem budget estimates of 51 Tg yr^{-1} of formic acid from photochemical oxidation and compared with estimates of 100−120 Tg yr^{-1} from observations.[68,69] Instead, HMHP acts as an intermediate species, producing formic acid further from emissions sources and resulting in higher formic acid mixing ratios in remote areas such as over the Atlantic Ocean. In contrast, the mixing ratios of HCHO are not significantly altered by inclusion of HMHP, as the model predicts only 0.1% of the total global annual HCHO production is due to HMHP oxidation, peaking at 1% of total local production in regions with high HMHP (see the Supporting Information). Note that the mixing ratios of HMHP presented in Figure 6A are likely an underestimate, as the ozonolysis of two important HMHP precursors, ethene and β-pinene, is not explicitly treated in the model. In addition, the contribution of HMHP oxidation to global formic acid concentrations is likely also a lower estimate. In these simulations, we assume that dry deposition represents a permanent loss of carbon from the atmosphere. If instead this process results in a flux of formic acid as suggested by Nguyen et al.[13], this would further increase the atmospheric concentrations of this carboxylic acid from HMHP.

CONCLUSIONS

The reaction rate constant from the HMHP + OH reaction shows that OH oxidation is a major loss process for HMHP in the atmosphere. Both OH reaction and, likely, dry deposition of HMHP lead to the formation of formic acid, a notable point given that models currently underestimate the concentration of atmospheric formic acid compared with measurements. Studies such as Paulot et al.[70] and Millet et al.[69] indicate that measured summertime boundary layer concentrations of formic acid can be more than double the model predicted values. These authors suggest that the discrepancy necessitates a 2−3 times larger source of formic acid than models currently contain, most likely in the form of formic acid production from secondary chemistry of biogenic and other chemical precursors. The results of this study further constrain the formic acid budget from a hydroperoxide that forms in the oxidation of a variety of biogenic and anthropogenic precursors and show that formic acid production from HMHP oxidation is not enough to account for the large discrepancy between models and observations. Additionally, given the importance of deposition to HMHP loss and potential for formic acid formation, this work highlights the need for improved understanding of surface chemistry.

ASSOCIATED CONTENT

Supporting Information

The Supporting Information is available free of charge on the ACS Publications website at DOI: 10.1021/acs.jpca.8b04577.

Calibration procedures; MC-TST and RRKM modeling details; GEOS-Chem modeling details (PDF)

AUTHOR INFORMATION

Corresponding Authors

*E-mail: hallen@caltech.edu (H.M.A.)

*E-mail: wennberg@caltech.edu (P.O.W.)

ORCID

John D. Crounse: 0000-0001-5443-729X

Kelvin H. Bates: 0000-0001-7544-9580

Jason M. St. Clair: 0000-0002-9367-5749

Kristian H. Møller: 0000-0001-8070-8516

Henrik G. Kjaergaard: 0000-0002-7275-8297

Paul O. Wennberg: 0000-0002-6126-3854

Notes

The authors declare no competing financial interest.

ACKNOWLEDGMENTS

This material is based upon work supported by the National Science Foundation Graduate Research Fellowship under Grant No. DGE-1144469; in addition, we acknowledge

DOI: 10.1021/acs.jpca.8b04577
J. Phys. Chem. A 2018, 122, 6292−6302

support from the NSF (Grant Nos. 1240604, 1628530, and 1628491) and NASA (Grants NNX12AC06G and NNX14AP46G). We acknowledge the Center for Exploitation of Solar Energy, University of Copenhagen, and the Danish Center for Scientific Computing for funding. We thank Daniel Jacob and the Atmospheric Chemistry Modeling Group at Harvard University for their work on the GEOS-Chem model. In addition, SEAC^{4}RS data from the Lidar Applications Group at the NASA Langley Research Center and from the Meteorological Measurement System (MMS) instrument operated by Paul Bui's group from the NASA Ames Research Center aided in the analysis presented here.

REFERENCES

(1) Jaeglé, L.; Jacob, D. J.; Wennberg, P. O.; Spivakovsky, C. M.; Hanisco, T. F.; Lanzendorf, E. J.; Hintsa, E. J.; Fahey, D. W.; Keim, E. R.; Proffitt, M. H.; et al. Observed OH and HO_2 in the upper troposphere suggest a major source from convective injection of peroxides. *Geophys. Res. Lett.* **1997**, *24*, 3181−3184.

(2) Jaeglé, L.; Jacob, D. J.; Brune, W. H.; Faloona, I.; Tan, D.; Heikes, B. G.; Kondo, Y.; Sachse, G. W.; Anderson, B.; Gregory, G. L.; et al. Photochemistry of HO_x in the upper troposphere at northern midlatitudes. *J. Geophys. Res.* **2000**, *105*, 3877−3892.

(3) Lee, M.; Heikes, B. G.; O'Sullivan, D. W. Hydrogen peroxide and organic hydroperoxide in the troposphere: a review. *Atmos. Environ.* **2000**, *34*, 3475−3494.

(4) Lind, J. A.; Lazrus, A. L.; Kok, G. L. Aqueous phase oxidation of sulfur(IV) by hydrogen peroxide, methylhydroperoxide, and peroxyacetic acid. *J. Geophys. Res.* **1987**, *92*, 4171−4177.

(5) Zhou, X.; Lee, Y.-N. Aqueous solubility and reaction kinetics of hydroxymethyl hydroperoxide. *J. Phys. Chem.* **1992**, *96*, 265−272.

(6) Marklund, S. The simultaneous determination of bis-(hydroxymethyl)peroxide (BHMP), hydroxymethylhydroproxide (HMP), and H_2O_2 with titanium(IV). Equilibria between the peroxides and the stabilities of HMP and BHMP at physiological conditions. *Acta Chem. Scand.* **1971**, *25*, 3517−3531.

(7) Hewitt, C. N.; Kok, G. L.; Fall, R. Hydroperoxides in plants exposed to ozone mediate air pollution damage to alkene emitters. *Nature* **1990**, *344*, 56−58.

(8) Sandermann, H. J.; Ernst, D.; Heller, W.; Langebartels, C. Ozone: an abiotic elicitor of plant defense reactions. *Trends Plant Sci.* **1998**, *3*, 47−50.

(9) Mehlhorn, H. Ethylene-promoted ascorbate peroxidase activity protects plants against hydrogen peroxide, ozone and paraquat. *Plant, Cell Environ.* **1990**, *13*, 971−976.

(10) Lee, J. H.; Leahy, D. F.; Tang, I. N.; Newman, L. Measurement and speciation of gas phase peroxides in the atmosphere. *J. Geophys. Res.* **1993**, *98*, 2911−2915.

(11) Fels, M.; Junkermann, W. The occurrence of organic peroxides in air at a mountain site. *Geophys. Res. Lett.* **1994**, *21*, 341−344.

(12) Weinstein-Lloyd, J. B.; Lee, J. H.; Daum, P. H.; Kleinman, L. I.; Nunnermacker, L. J.; Springston, S. R.; Newman, L. Measurements of peroxides and related species during the 1995 summer intensive of the Southern Oxidants Study in Nashville, Tennessee. *J. Geophys. Res.* **1998**, *103*, 22361−22373.

(13) Nguyen, T. B.; Crounse, J. D.; Teng, A. P.; St. Clair, J. M.; Paulot, F.; Wolfe, G. M.; Wennberg, P. O. Rapid deposition of oxidized biogenic compounds to a temperate forest. *Proc. Natl. Acad. Sci. U. S. A.* **2015**, *112*, E392−E401.

(14) Qi, B.; Chao, Y. T.; Chen, Z. M. Mechanism and kinetics of the production of hydroxymethyl hydroperoxide in ethene/ozone/water gas-phase system. *Sci. China, Ser. B: Chem.* **2007**, *50*, 425−431.

(15) Crehuet, R.; Anglada, J. M.; Bofill, J. M. Tropospheric formation of hydroxymethyl hydroperoxide, formic acid, H_2O_2, and OH from carbonyl oxide in the presence of water vapor: a theoretical study of the reaction mechanism. *Chem. - Eur. J.* **2001**, *7*, 2227−2235.

(16) Gäb, S.; Hellpointner, E.; Turner, W. V.; Korte, F. Hydroxymethyl hydroperoxide and bis(hydroxymethyl) peroxide from gas-phase ozonolysis of naturally occuring alkenes. *Nature* **1985**, *316*, 535−536.

(17) Horie, O.; Neeb, P.; Limbach, S.; Moortgat, G. K. Formation of formic acid and organic peroxides in the ozonolysis of ethene with added water vapour. *Geophys. Res. Lett.* **1994**, *21*, 1523−1526.

(18) Huang, D.; Chen, Z. M.; Zhao, Y.; Liang, H. Newly observed peroxides and the water effect on the formation and removal of hydroxyalkyl hydroperoxides in the ozonolysis of isoprene. *Atmos. Chem. Phys.* **2013**, *13*, 5671−5683.

(19) Sauer, F.; Schäfer, C.; Neeb, P.; Horie, O.; Moortgat, G. K. Formation of hydrogen peroxide in the ozonolysis of isoprene and simple alkenes under humid conditions. *Atmos. Environ.* **1999**, *33*, 229−241.

(20) Nakajima, M.; Endo, Y. Observation of hydroxymethyl hydroperoxide in a reaction system containing CH_2OO and water vapor through pure rotational spectroscopy. *J. Chem. Phys.* **2015**, *143*, 164307.

(21) Su, F.; Calvert, J. G.; Shaw, J. H. Mechanism of the photooxidation of gaseous formaldehyde. *J. Phys. Chem.* **1979**, *83*, 3185−3191.

(22) Bauerle, S.; Moortgat, G. K. Absorption cross-sections of $HOCH_2OOH$ vapor between 205 and 360 nm at 298 K. *Chem. Phys. Lett.* **1999**, *309*, 43−48.

(23) Fry, J. L.; Matthews, J.; Lane, J. R.; Roehl, C. M.; Sinha, A.; Kjaergaard, H. G.; Wennberg, P. O. OH-stretch vibrational spectroscopy of hydroxymethyl hydroperoxide. *J. Phys. Chem. A* **2006**, *110*, 7072−7079.

(24) Roehl, C. M.; Marka, Z.; Fry, J. L.; Wennberg, P. O. Near-UV photolysis cross sections of CH_3OOH and $HOCH_2OOH$ determined via action spectroscopy. *Atmos. Chem. Phys.* **2007**, *7*, 713−720.

(25) Eisfeld, W.; Francisco, J. S. Excited states and photodissociation of hydroxymethyl hydroperoxide. *J. Chem. Phys.* **2008**, *128*, 174304.

(26) O'Sullivan, D. W.; Lee, M.; Noone, B. C.; Heikes, B. G. Henry's law constant determinations for hydrogen peroxide, methyl hydroperoxide, hydroxymethyl hydroperoxide, ethyl hydroperoxide, and peroxyacetic acid. *J. Phys. Chem.* **1996**, *100*, 3241−3247.

(27) Francisco, J. S.; Eisfeld, W. Atmospheric oxidation mechanism of hydroxymethyl hydroperoxide. *J. Phys. Chem. A* **2009**, *113*, 7593−7600.

(28) Crounse, J. D.; McKinney, K. A.; Kwan, A. J.; Wennberg, P. O. Measurement of gas-phase hydroperoxides by chemical ionization mass spectrometry. *Anal. Chem.* **2006**, *78*, 6726−6732.

(29) Paulot, F.; Crounse, J. D.; Kjaergaard, H. G.; Kroll, J. H.; Seinfeld, J. H.; Wennberg, P. O. Isoprene photooxidation: new insights into the production of acids and organic nitrates. *Atmos. Chem. Phys.* **2009**, *9*, 1479−1501.

(30) St. Clair, J. M.; McCabe, D. C.; Crounse, J. D.; Steiner, U.; Wennberg, P. O. Chemical ionization tandem mass spectrometer for the in situ measurement of methyl hydrogen peroxide. *Rev. Sci. Instrum.* **2010**, *81*, 094102.

(31) Cazorla, M.; Wolfe, G. M.; Bailey, S. A.; Swanson, A. K.; Arkinson, H. L.; Hanisco, T. F. A new airborne laser-induced fluorescence instrument for in situ detection of formaldehyde throughout the troposphere and lower stratosphere. *Atmos. Meas. Tech.* **2015**, *8*, 541−552.

(32) Bates, K. H.; Nguyen, T. B.; Teng, A. P.; Crounse, J. D.; Kjaergaard, H. G.; Stoltz, B. M.; Seinfeld, J. H.; Wennberg, P. O. Production and fate of C_4 dihydroxycarbonyl compounds from isoprene oxidation. *J. Phys. Chem. A* **2016**, *120*, 106−117.

(33) Praske, E.; Crounse, J. D.; Bates, K. H.; Kurtén, T.; Kjaergaard, H. G.; Wennberg, P. O. Atmospheric fate of methyl vinyl ketone: Peroxy radical reactions with NO and HO_2. *J. Phys. Chem. A* **2015**, *119*, 4562−4572.

(34) Teng, A. P.; Crounse, J. D.; Lee, L.; St. Clair, J. M.; Cohen, R. C.; Wennberg, P. O. Hydroxy nitrate production in the OH-initiated oxidation of alkenes. *Atmos. Chem. Phys.* **2015**, *15*, 4297−4316.

(35) Taylor, W. D.; Allston, T. D.; Moscato, M. J.; Fazekas, G. B.; Kozlowski, R.; Takacs, G. A. Atmospheric photo-dissociation lifetimes

DOI: 10.1021/acs.jpca.8b04577
J. Phys. Chem. A 2018, 122, 6292−6302

for nitromethane, methyl nitrite, and methyl nitrate. *Int. J. Chem. Kinet.* **1980**, *12*, 231−240.
(36) Su, T.; Chesnavich, W. J. Parameterization of the ion-polar molecule collision rate constant by trajectory calculations. *J. Chem. Phys.* **1982**, *76*, 5183−5183.
(37) Garden, A. L.; Paulot, F.; Crounse, J. D.; Maxwell-Cameron, I. J.; Wennberg, P. O.; Kjaergaard, H. G. Calculation of conformationally weighted dipole moments useful in ion−molecule collision rate estimates. *Chem. Phys. Lett.* **2009**, *474*, 45−50.
(38) Paulot, F.; Crounse, J. D.; Kjaergaard, H. G.; Kroll, J. H.; Seinfeld, J. H.; Wennberg, P. O. Isoprene photooxidation: new insights into the production of acids and organic nitrates. *Atmos. Chem. Phys.* **2009**, *9*, 1479−1501.
(39) Møller, K. H.; Otkjær, R. V.; Hyttinen, N.; Kurtén, T.; Kjaergaard, H. G. Cost-effective implementation of multiconformer transition state theory for peroxy radical hydrogen shift reactions. *J. Phys. Chem. A* **2016**, *120*, 10072−10087.
(40) Werner, H.-J.; Knowles, P. J.; Knizia, G.; Manby, F. R.; Schütz, M.; Celani, P.; Györffy, W.; Kats, D.; Korona, T.; Lindh, R. et al.. *MOLPRO, a package of ab initio programs*, version 2012.1; 2012; see http://www.molpro.net.
(41) Frisch, M. J.; Trucks, G. W.; Schlegel, H. B.; Scuseria, G. E.; Robb, M. A.; Cheeseman, J. R.; Scalmani, G.; Barone, V.; Mennucci, B.; Petersson, G. A.; Nakatsuji, H.; Caricato, M.; Li, X.; Hratchian, H. P.; Izmaylov, A. F.; Bloino, J.; Zheng, G.; Sonnenberg, J. L.; Hada, M.; Ehara, M.; Toyota, K.; Fukuda, R.; Hasegawa, J.; Ishida, M.; Nakajima, T.; Honda, Y.; Kitao, O.; Nakai, H.; Vreven, T.; Montgomery, J. A., Jr.; Peralta, J. E.; Ogliaro, F.; Bearpark, M.; Heyd, J. J.; Brothers, E.; Kudin, K. N.; Staroverov, V. N.; Kobayashi, R.; Normand, J.; Raghavachari, K.; Rendell, A.; Burant, J. C.; Iyengar, S. S.; Tomasi, J.; Cossi, M.; Rega, N.; Millam, J. M.; Klene, M.; Knox, J. E.; Cross, J. B.; Bakken, V.; Adamo, C.; Jaramillo, J.; Gomperts, R.; Stratmann, R. E.; Yazyev, O.; Austin, A. J.; Cammi, R.; Pomelli, C.; Ochterski, J. W.; Martin, R. L.; Morokuma, K.; Zakrzewski, V. G.; Voth, G. A.; Salvador, P.; Dannenberg, J. J.; Dapprich, S.; Daniels, A. D.; Farkas, O.; Foresman, J. B.; Ortiz, J. V.; Cioslowski, J.; Fox, D. J. *Gaussian 09*, revision D.01; Gaussian, Inc.: Wallingford, CT, 2009.
(42) Glowacki, D. R.; Liang, C.-H.; Morley, C.; Pilling, M. J.; Robertson, S. H. MESMER: An open-source master equation solver for multi-energy well reactions. *J. Phys. Chem. A* **2012**, *116*, 9545−9560.
(43) Barker, J. R.; Nguyen, T. L.; Stanton, J. F.; Aieta, C.; Ceotto, M.; Gabas, F.; Kumar, T. J. D.; Li, C. G. L.; Lohr, L. L.; Maranzana, A. et al. *MultiWell-2017 Program Suite*; University of Michigan: Ann Arbor, MI, USA; 2017.
(44) Bethel, H. L.; Atkinson, R.; Arey, J. Kinetics and products of the reactions of selected diols with the OH radical. *Int. J. Chem. Kinet.* **2001**, *33*, 310−316.
(45) York, D.; Evensen, N. M.; Martínez, M. L.; De Basabe Delgado, J. Unified equations for the slope, intercept, and standard errors of the best straight line. *Am. J. Phys.* **2004**, *72*, 367−375.
(46) Sander, S. P.; Abbatt, J.; Barker, J. R.; Burkholder, J. B.; Friedl, R. R.; Golden, D. M.; Huie, R. E.; Kolb, C. E.; Kurylo, M. J.; Moortgat, G. K. et al.. *Chemical kinetics and photochemical data for use in atmospheric studies, evaluation no. 17*; JPL Publication 10−6; Jet Propulsion Laboratory, Pasadena, CA, USA, 2011.
(47) Atkinson, R.; Aschmann, S. M.; Carter, W. P. L.; Winer, A. M.; Pitts, J. N. Alkyl nitrate formation from the NO_X -air photooxidations of C_2−C_8 n-alkanes. *J. Phys. Chem.* **1982**, *86*, 4563−4569.
(48) Hasson, A. S.; Orzechowska, G.; Paulson, S. E. Production of stabilized Criegee intermediates and peroxides in the gas phase ozonolysis of alkenes: 1. ethene, trans-2-butene, and 2,3-dimethyl-2-butene. *J. Geophys. Res.* **2001**, *106*, 34131−34142.
(49) Veyret, B.; Roussel, P.; Lesclaux, R. Mechanism of the chain process forming H_2 in the photooxidation of formaldehyde. *Int. J. Chem. Kinet.* **1984**, *16*, 1599−1608.
(50) Henon, E.; Bohr, F.; Sokolowski-Gomez, N.; Caralp, F. Degradation of three oxygenated alkoxy radicals of atmospheric interest: $HOCH_2O^{\cdot}$, $CH_3OCH_2O^{\cdot}$, $CH_3OCH_2OCH_2O^{\cdot}$, RRKM theoretical study of the β-C-H bond scission and the 1,6-isomerisation kinetics. *Phys. Chem. Chem. Phys.* **2003**, *5*, 5431−5437.
(51) Atkinson, R. Gas-phase tropospheric chemistry of organic compounds: A review. *Atmos. Environ.* **2007**, *41*, 200−240.
(52) Veyret, B.; Rayez, J.-C.; Lesclaux, R. Mechanism of the photooxidation of formaldehyde studied by flash photolysis of CH_2O-O_2-NO mixtures. *J. Phys. Chem.* **1982**, *86*, 3424−3430.
(53) Barnes, I.; Becker, K. H.; Fink, E. H.; Reimer, A.; Zabel, F.; Niki, H. FTIR spectroscopic study of the gas-phase reaction of HO_2 with H_2CO. *Chem. Phys. Lett.* **1985**, *115*, 1−8.
(54) Veyret, B.; Lesclaux, R.; Rayez, M.-T.; Rayez, J. C.; Cox, R. A.; Moortgat, G. K. Kinetics and mechanism of the photooxidation of formaldehyde. 1. Flash photolysis study. *J. Phys. Chem.* **1989**, *93*, 2368−2374.
(55) Burrows, J. P.; Moortgat, G. K.; Tyndall, G. S.; Cox, R. A.; Jenkin, M. E.; Hayman, G. D.; Veyret, B. Kinetics and mechanism of the photooxidation of formaldehyde: 2. Molecular modulation studies. *J. Phys. Chem.* **1989**, *93*, 2375−2382.
(56) Hermans, I.; Müller, J.-F.; Nguyen, T. L.; Jacobs, P. A.; Peeters, J. Kinetics of α-hydroxy-alkylperoxyl radicals in oxidation processes. $HO_2^{\cdot}$-initiated oxidation of ketones/aldehydes near the tropopause. *J. Phys. Chem. A* **2005**, *109*, 4303−4311.
(57) Morajkar, P.; Schoemaecker, C.; Okumura, M.; Fittschen, C. Direct measurement of the equilibrium constants of the reaction of formaldehyde and acetaldehyde with HO_2 radicals. *Int. J. Chem. Kinet.* **2014**, *46*, 245−259.
(58) Vaghjiani, G. L.; Ravishankara, A. R. Kinetics and mechanism of OH reaction with CH_3OOH. *J. Phys. Chem.* **1989**, *93*, 1948−1959.
(59) Feiner, P. A.; Brune, W. H.; Miller, D. O.; Zhang, L.; Cohen, R. C.; Romer, P. S.; Goldstein, A. H.; Keutsch, F. N.; Skog, K. M.; Wennberg, P. O.; et al. Testing atmospheric oxidation in an Alabama forest. *J. Atmos. Sci.* **2016**, *73*, 4699−4710.
(60) Bey, I.; Jacob, D. J.; Yantosca, R. M.; Logan, J. A.; Field, B. D.; Fiore, A. M.; Li, Q.; Liu, H. Y.; Mickley, L. J.; Schultz, M. G. Global modeling of tropospheric chemistry with assimilated meteorology: Model description and evaluation. *J. Geophys. Res.* **2001**, *106*, 23073−23095.
(61) Mao, J.; Paulot, F.; Jacob, D. J.; Cohen, R. C.; Crounse, J. D.; Wennberg, P. O.; Keller, C. A.; Hudman, R. C.; Barkley, M. P.; Horowitz, L. W. Ozone and organic nitrates over the eastern United States: Sensitivity to isoprene chemistry. *J. Geophys. Res. Atmos.* **2013**, *118*, 11256−11268.
(62) St. Clair, J. M.; Rivera-Rios, J. C.; Crounse, J. D.; Knap, H. C.; Bates, K. H.; Teng, A. P.; Jørgensen, S.; Kjaergaard, H. G.; Keutsch, F. N.; Wennberg, P. O. Kinetics and products of the reaction of the first-generation isoprene hydroxy hydroperoxide (ISOPOOH) with OH. *J. Phys. Chem. A* **2016**, *120*, 1441−1451.
(63) Nguyen, T. B.; Tyndall, G. S.; Crounse, J. D.; Teng, A. P.; Bates, K. H.; Schwantes, R. H.; Coggon, M. M.; Zhang, L.; Feiner, P.; Miller, D. O.; et al. Atmospheric fates of Criegee intermediates in the ozonolysis of isoprene. *Phys. Chem. Chem. Phys.* **2016**, *18*, 10241.
(64) Bates, K. H.; Crounse, J. D.; St. Clair, J. M.; Bennett, N. B.; Nguyen, T. B.; Seinfeld, J. H.; Stoltz, B. M.; Wennberg, P. O. Gas phase production and loss of isoprene epoxydiols. *J. Phys. Chem. A* **2014**, *118*, 1237−1246.
(65) Teng, A. P.; Crounse, J. D.; Wennberg, P. O. Isoprene peroxy radical dynamics. *J. Am. Chem. Soc.* **2017**, *139*, 5367−5377.
(66) Neeb, P.; Sauer, F.; Horie, O.; Moortgat, G. K. Formation of hydroxymethyl hydroperoxide and formic acid in alkene ozonolysis in the presence of water vapour. *Atmos. Environ.* **1997**, *31*, 1417−1423.
(67) Hasson, A. S.; Ho, A. W.; Kuwata, K. T.; Paulson, S. E. Production of stabilized Criegee intermeidates and peroxides in the gas phase ozonolysis of alkenes: 2. asymmetric and biogenic alkenes. *J. Geophys. Res.* **2001**, *106*, 34143−34153.
(68) Stavrakou, T.; Müller, J.-F.; Peeters, J.; Razavi, A.; Clarisse, L.; Clerbaux, C.; Coheur, P.-F.; Hurtmans, D.; De Maziére, M.; Vigouroux, C.; et al. Satellite evidence for a large source of formic acid from boreal and tropical forests. *Nat. Geosci.* **2012**, *5*, 26−30.

DOI: 10.1021/acs.jpca.8b04577
J. Phys. Chem. A 2018, 122, 6292−6302

(69) Millet, D. B.; Baasandorj, M.; Farmer, D. K.; Thornton, J. A.; Baumann, K.; Brophy, P.; Chaliyakunnel, S.; de Gouw, J. A.; Graus, M.; Hu, L.; et al. A large and ubiquitous source of atmospheric formic acid. *Atmos. Chem. Phys.* **2015**, *15*, 6283−6304.
(70) Paulot, F.; Wunch, D.; Crounse, J. D.; Toon, G. C.; Millet, D. B.; DeCarlo, P. F.; Vigouroux, C.; Deutscher, N. M.; González Abad, G.; Notholt, J.; et al. Importance of secondary sources in the atmospheric budgets of formic and acetic acids. *Atmos. Chem. Phys.* **2011**, *11*, 1989−2013.

DOI: 10.1021/acs.jpca.8b04577
J. Phys. Chem. A 2018, 122, 6292−6302